AIAA JOURNAL
Vol. 56, No. 10, October 2018

Circulation Redistribution in Leading-Edge Vortices with Spanwise Flow

Jaime G. Wong,* Graeme Gillespie,† and David E. Rival‡
Queen's University, Kingston, Ontario K7L 3N6, Canada

DOI: 10.2514/1.J057030

A low-order model for the circulation budget within a leading-edge vortex (LEV) is proposed, based on one-dimensional species advection. The model is composed of two parts: first, a shear-layer model predicts the circulation feeding rate into the LEV; and second, a spanwise transport model initializes vorticity-containing mass with a finite circulation, allowing circulation to advect along the span with spanwise flow. No empirical data are necessary to inform the results of the model. As a proof of concept, both components of the proposed model are evaluated against a flat-plate delta wing. Using particle image velocimetry, the proposed shear-layer model is found to predict circulation flux into the LEV. Particle-tracking velocimetry is used to validate the spanwise transport of circulation. By allowing a vorticity-containing mass to advect with the spanwise flow, the model automatically satisfies the vorticity transport equation when vortex tilting and viscous diffusion are neglected. Neglecting the vortex tilting and viscous diffusion terms results in an error of approximately 10% of the spanwise advection, such that these terms are within the acceptable tolerance of a low-cost model. Thus, the proposed model is a computationally inexpensive tool for predicting circulation redistribution in flows with specific three-dimensional effects, providing a framework for broader parameter studies going forward.

Nomenclature

c	=	wing chord
d	=	shear-layer thickness
k	=	reduced frequency
l	=	shear-layer length
m'	=	mass (per unit span)
N	=	number of bins (discretization in span)
St	=	Strouhal number
t	=	time
U_∞	=	freestream velocity
u_{eff}	=	effective velocity
u_i	=	inner shear-layer velocity
u_o	=	outer shear-layer velocity
w	=	spanwise flow
X, Y, Z	=	global coordinate system
z	=	spanwise direction
α	=	angle of attack
α_o	=	geometric angle of attack
Γ	=	circulation
Λ	=	sweep angle
ξ	=	shear-layer coordinate
ρ	=	density
ω	=	vorticity

Subscripts

i	=	index in time
k	=	index in span

I. Introduction

THE rapid flapping motion of an insect wing produces a strong and compact leading-edge vortex (LEV) [1]. Such structures are also found in fish and bird locomotion [2,3], as well as both of their engineering analogs of autonomous underwater vehicles and micro aerial vehicles, respectively. Although the investigation of the LEV in relation to biological locomotion has received significant attention since the mid-1990s [1], similar LEVs have been of engineering interest on delta wings for many decades [4]. In each of these aforementioned cases, the LEV develops in the pattern illustrated by Fig. 1: vorticity formed in a leading-edge shear layer is fed into the vortex and, if spanwise flow exists, that vorticity may be advected along the leading edge in the outboard direction.

An LEV that forms on a nominally two-dimensional profile with no spanwise flow will always eventually detach and convect downstream because there is no vorticity sink [5]. For such a case, the development of an LEV on a pitching or heaving profile is influenced by a small number of parameters, such as the reduced frequency k or Strouhal number St [6–9]. In particular, the Strouhal number St determines force generation, whereas the reduced frequency k dominates the flow topology and the eventual detachment of the LEV. In turn, when the circulation of an LEV is normalized by its feeding shear-layer velocity, the circulation is not affected by reduced frequency [10]. A very large reduced frequency k represents a very fast motion as compared to the development time of the LEV; subsequently, the LEV never grows large enough to detach before the end of a motion. Several very powerful methods exist for predicting the development of the LEV in two-dimensional cases for arbitrary motions, especially using discrete vortex methods [11,12]. However, these two-dimensional cases represent only a small subset of the LEVs that are observed in engineering practice.

A canonical three-dimensional LEV is formed on a delta wing, as shown in Fig. 1. This LEV would rapidly saturate and detach if the vorticity-containing mass was not advected away along the span of the profile. This same physics governs LEV formation in biological and bioinspired swimmers and flyers, in which leading-edge curvature and centrifugal accelerations are used to manipulate circulation [13] and mass transport [14]. For instance, similar lunate tail fins have evolved in several species of swimmers of distinct evolutionary lineage [13], whereas the pronounced leading-edge curvature of common swifts is used to form a stable LEV [2]. However, in a study of swept wings at sweep angles of up to $\Lambda = 45$ deg, leading-edge shape alone was found to be insufficient to stabilize an LEV [15]. Both the spanwise advection of vorticity and the annihilation of vorticity are critical circulation-regulating mechanisms [9,16]. The spanwise advection of vorticity is especially difficult to account for because most models for LEV growth are explicitly two-dimensional, such as the strip-theory approaches [17].

Received 11 January 2018; revision received 24 April 2018; accepted for publication 19 June 2018; published online 31 July 2018.

*Graduate Student, Department of Mechanical and Materials Engineering.
†Undergraduate Student, Department of Mechanical and Materials Engineering.
‡Associate Professor, Department of Mechanical and Materials Engineering.

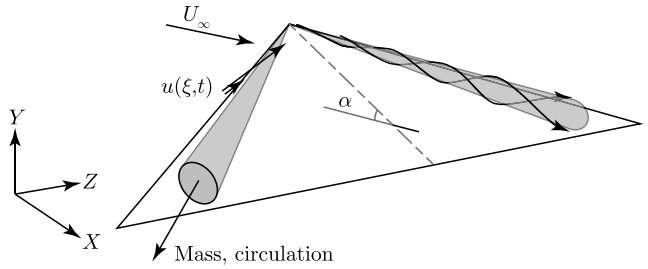

Fig. 1 Schematic diagram of the vortex structure on a delta wing.

Therefore, the current study provides a model appropriate for both engineering practice and in the study of biologically inspired flows by explicitly accounting for this spanwise circulation transport.

A computationally inexpensive model for LEV growth in the presence of spanwise flow is presented here. This model is derived in the following section, based on a numerical simulation of the advection of a vorticity-containing mass along the span of a profile. To provide a proof of concept with which to inform future parameter studies, a canonical LEV is produced experimentally using a nonslender flat-plate delta wing, as described in Sec. III. However, it should be noted that this model is also applicable to biological and bioinspired flows.

II. One-Dimensional Numerical Simulation of Circulation Transport

Previous modeling efforts have suffered from either limited three-dimensional information or a dependence on empirical data, such as shear-layer thickness or velocity [18]. The proposed model attempts to solve these limitations by treating circulation transport as species transport, in which the circulation follows the flow of mass through the domain. Such a model requires the assumptions of limited vortex tilting and large advection relative to the diffusion of vorticity. This model is divided into two parts: the feeding of circulation through a shear layer, and the subsequent transport of that circulation along the span of a profile.

Determining the growth of a vortex based on its shear-layer properties is a classical technique [19]. Previous work has applied this technique to LEV growth to give the circulation feeding rate of an LEV as follows:

$$\frac{\partial \Gamma}{\partial t} \propto u_{\text{eff}}^2 \tag{1}$$

where u_{eff} is the effective velocity of the profile at the leading edge [9]. This solution has the same form as that determined for vortex rings formed on piston cylinders [20]. The constant of proportionality depends on the shape of the velocity profile in the shear layer. More precisely, this expression for shear-layer feeding can be expanded as follows:

$$\frac{\partial \Gamma}{\partial t} = \frac{\partial \Gamma}{\partial m'}\frac{\partial m'}{\partial t} \tag{2}$$

where m' is the mass per unit span at a location of interest. Following the diagram of the shear layer in Fig. 2, the mass rate into the LEV of $\partial m'/\partial t$ can be computed by integration of the shear-layer velocity profile highlighted by the red circle in the figure. Moreover, the circulation in the shear layer can be computed by path integration to be $\Gamma = u_o l$, where u_o is the outer shear-layer velocity and the inner shear-layer velocity u_i is neglected. The outer shear-layer velocity u_o is typically greater than the effective velocity due to the acceleration effect around the LEV. Meanwhile, the mass inside the shear layer (per unit span) is $\rho d l$. Thus, we can insert specific values into Eq. (2) so as to obtain the following:

$$\frac{\partial \Gamma}{\partial m'}\frac{\partial m'}{\partial t} = \left(\frac{u_o l}{\rho d l}\right)\left(\frac{1}{2}(u_o + u_i)\rho d\right) = \frac{1}{2}(u_o^2 + u_o u_i) \tag{3}$$

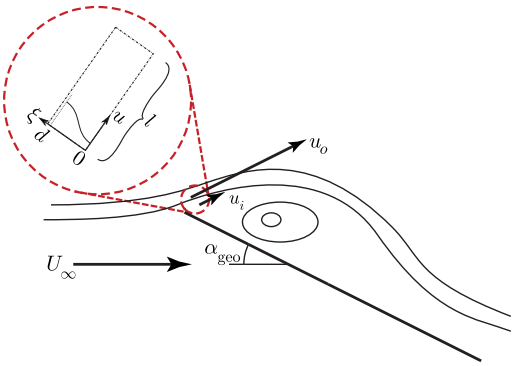

Fig. 2 Cross-sectional view of a vortex growing on a flat plate, where ξ is the coordinate across the shear layer.

where u_i is the inner shear-layer velocity, which is assumed to be zero. Setting $u_i = 0$ gives a circulation feeding rate of

$$\frac{\partial \Gamma}{\partial t} = \frac{1}{2}u_o^2 \tag{4}$$

Previous studies of vortex rings formed by piston cylinders have also determined this relationship between vortex strength and shear-layer velocity [20]. Therefore, we need only to compute the outer shear-layer velocity in order to estimate the flux of vorticity into the LEV. It should be noted that, for any dynamic motion (for instance, in biological or bioinspired profile motions), the appropriate scaling velocity for the shear layer is the local effective velocity u_{eff} and not the freestream velocity U_∞ [21]. In future studies, this may allow for the extension of the aforementioned model to include unsteady biological and bioinspired locomotion modes, in addition to delta wings and rotating machinery. However, for the purposes of the proof of concept in this study, the shear-layer velocity will be assumed as $u_o = U_\infty$. Real shear-layer velocities are a complex function of many factors, including angle of attack. The freestream velocity is nevertheless chosen here as the minimum-cost option for demonstrating the functionality of the model. However, future studies may need to account for this higher shear-layer velocity.

The assumption that circulation follows fluid mass in the flow is valid for flows with small vortex tilting and viscous diffusion. For nominally two-dimensional flows, LEV circulation is regulated primarily by vorticity annihilation, and vorticity convection is small [18,22]. Therefore, the following analysis is specific to a limited subset of three-dimensional flows in which vortex tilting and viscous diffusion are small. Although this dramatically simplifies the analysis of circulation transport, it still requires the computation of mass transport within the flow. Estimating mass transport explicitly would require empirical values such as the shear-layer thickness, which should ideally be avoided. A solution to this problem is proposed here, in which mass transport is used conceptually in the following derivation; but, by focusing on circulation as the model output, empirical parameters such as shear-layer thickness are eliminated before the final output is computed.

At each time step, particles are initialized in a uniform distribution along the spanwise domain of the profile, as shown in Fig. 3a. As there are no particles before the first time step, this implicitly sets the initial conditions as $\Gamma = 0$ everywhere. An alternative initial condition can be set by initializing a virtual time step with the desired circulation distribution. This spanwise domain is discretized into i bins, with each representing one spanwise slice that is treated locally as two-dimensional. The circulation generated at that spanwise slice of $\Delta\Gamma = (1/2)u_o^2\Delta t$ is divided equally among all the N particles in that domain. Thus, every particle is initialized with the circulation:

$$\Gamma_k = \frac{1}{2N}u_o^2\Delta t \tag{5}$$

where N is the number of particles in a particular bin i. In the current study, the shear-layer velocity u_o is uniform; but, for flapping or

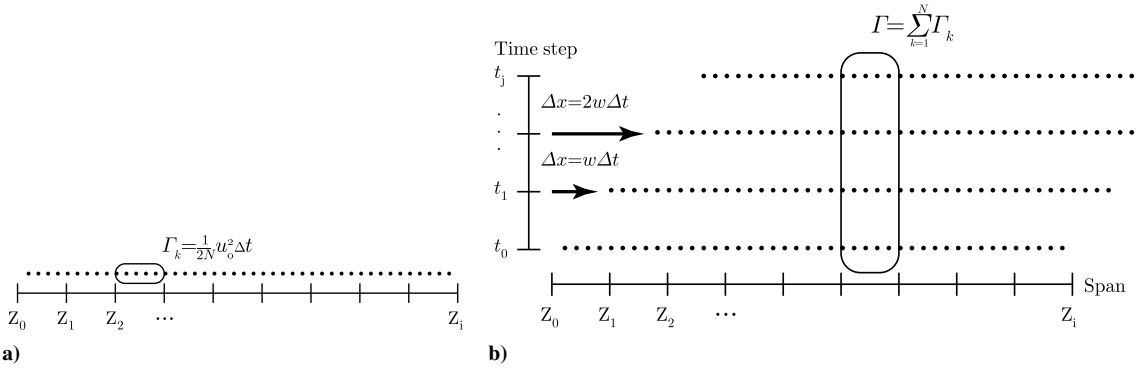

Fig. 3 Visualization of how a) circulation generation is represented within the simulation and b) total circulation is calculated at a given time step.

rotating profiles, it may vary as a function of span. These particles are assumed to retain their initial circulation. This assumption is equivalent to assuming that circulation transport follows regular species transport.

Spanwise flow is accounted for by advecting these particles through the domain at the spanwise velocity, as shown in Fig. 3b. This avoids the difficult task of determining an explicit boundary condition for the circulation Γ or the gradient of circulation. Thus, at each time step j, the circulation for a spanwise location z_i is the sum of the elemental circulation of all the particles generated at that location and time step, plus the circulation of particles initialized at prior time steps that advected to that spanwise location:

$$\Gamma(z_i) = \sum_{k=1}^{N} \Gamma_k \tag{6}$$

As an example, consider a delta wing with a sweep angle of $\Lambda = 45$ deg travelling at a constant velocity U_∞. The component of the freestream velocity U_∞ parallel to the wing span is $U_\infty/\sqrt{2}$. As a first approximation, we can assume that the mean spanwise flow $\bar{w}$ in the LEV is the average of this freestream flow and the zero-flow velocity at the wall of the wing. With this assumption, the mean spanwise flow will be $\bar{w} = U_\infty/(2\sqrt{2})$. The resulting spatially and temporally resolved circulation distribution is shown in Fig. 4, normalized for a chord of c. As one would expect, the circulation distribution rapidly approaches a steady value, with a linearly increasing circulation toward the profile tip.

The quality of the circulation distribution shown in Fig. 4 can be inspected using the vorticity transport equation. By integrating the vorticity transport equation, the circulation advection out of the vortex is given by the following:

$$\frac{\partial \Gamma}{\partial t} = \bar{w}\frac{\partial \Gamma}{\partial z} \tag{7}$$

where $\bar{w}$ is the mean spanwise flow [9]. We can then add the rate of circulation entering the LEV, given in Eq. (4), to this rate of circulation exiting the LEV given in Eq. (7):

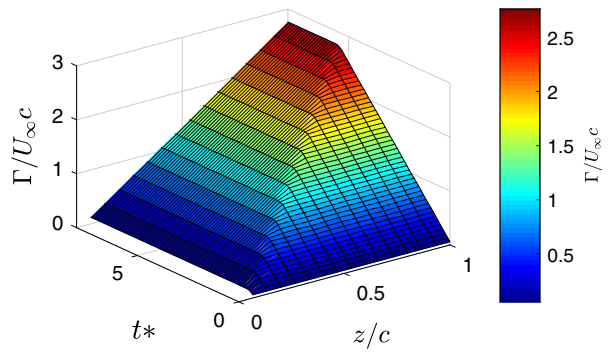

Fig. 4 Example of the spatial and temporal circulation distribution computed by the proposed model for a delta wing.

$$\frac{\partial \Gamma}{\partial t_{\text{tot}}} = \frac{\partial \Gamma}{\partial t_{\text{in}}} - \frac{\partial \Gamma}{\partial t_{\text{out}}} = \frac{1}{2}u_o^2 - \bar{w}\frac{\partial \Gamma}{\partial z} \tag{8}$$

For an LEV in steady state, the rate of change of circulation can be set to zero and Eq. (8) can be rearranged to yield an expected circulation gradient for an LEV in steady state:

$$\frac{\partial \Gamma}{\partial z} = \frac{(1/2)u_o^2}{w} \tag{9}$$

When the circulation gradient $\partial\Gamma/\partial z$ that is produced by the preceding model is inspected, we find that it satisfies the preceding equation within 0.1%, meaning that all of the circulation that enters the vortex is being advected along the span, aside from small numerical error. In this way, the numerical simulation is satisfying the vorticity transport equation simply by advecting circulation along the span with spanwise flow. To provide further proof of concept, the model presented previously can be compared to an experimental test case, as will be described in the following section.

III. Experimental Methods

A single experimental test case is presented here as a proof of concept of the aforementioned numerical simulation. A nonslender flat-plate delta wing with a sweep angle of $\Lambda = 45$ deg is used here as a canonical test case because it exhibits a strong, stationary LEV that can be easily characterized by optical measurements. This delta wing is investigated in the 15 m-long optical towing tank at Queen's University, as shown in Fig. 5. The towing tank has a 1×1 m^2 cross section, with optical access through both side walls and the floor; whereas the partially enclosed roof section mitigates surface waves. A high-speed rack-and-pinion traverse was used to tow the delta wing, which was mounted to a sting via the pressure side of the profile. A geometric angle of attack of $\alpha_{\text{geo}} = 20$ deg was used for all measurements, and the delta wing was towed at a velocity of $U_\infty = 0.875$ m/s, corresponding to a Reynolds number of $Re = 260{,}000$. The resulting flowfields were captured with two different measurement techniques in order to characterize the small-scale shear layer and large-scale circulation transport, which will be described in the following two sections, respectively.

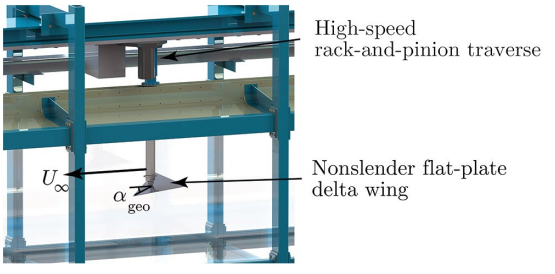

Fig. 5 Schematic of the test article in the towing tank.

A. High-Speed Shear-Layer Measurements

To test the shear-layer feeding model, high-speed planar particle image velocimetry (two-dimensional particle image velocimetry) measurements are conducted over a very small field of view (FOV), as shown in Fig. 6a. This field of view is approximately 30×30 mm^2, illuminated with a 527 nm Photonics Industries 40 mJ per pulse neodymium-doped yttrium lithium fluoride (Nd:YLF) laser. This field of view is placed halfway between the apex of the delta wing and the wing tip. The laser is used to illuminate 100 μm hollow glass microspheres seeded into the flow, which are tracked with a Photron SA-Z high-speed camera operating at 10,000 Hz at a resolution of 1024×1024 pixel^2. A single run of data is used to produce the shear-layer measurements. However, data from 200 successive time steps are cast into the plate-fixed coordinate frame and averaged in order to produce the final vector field.

B. Spanwise-Resolved Circulation Advection Measurements

Four-dimensional particle-tracking velocimetry (4-D-PTV) [23] is used to capture the vorticity transport properties of the vortex above the flat-plate delta wing, using the same seeding particles and illumination as the particle image velocimetry (PIV) experiments, illustrated in Fig. 6b. The volumetric time-resolved data are necessary in order to measure the gradients of circulation along the span. The FOV is $120 \times 120 \times 10$ mm^3, at the same location as for PIV. The 10 mm spanwise extent of the imaged volume is approximately 3.5% of the semispan of the delta wing. Images are captured with four Photron SA-4 cameras operated at 1500 Hz at a resolution of 1024×1024 pixel^2. Once again, a single run is used to characterize the vorticity transport within the domain, in which data from 50 adjacent frames are cast into the plate-fixed coordinate frame and averaged in order to produce the final vector field. The 4-D-PTV algorithm used in this study is implemented in LaVision Davis 8.3.0 software. The 4-D-PTV has been shown to have a triangulation error of approximately half that of tomographic PIV, with triangulation errors of 0.01–0.02 pixels at similar seeding densities to those in the current study [23].

IV. Results and Discussion

The small-scale PIV measurements are shown in Fig. 7 for both the velocity and vorticity fields. The black lines shown in Fig. 7a are used to sample the effective velocity u_{eff}/U_∞, which can be compared to the values used in the numerical simulations. Meanwhile, the black lines in Fig. 7b are used to sample $u_x\omega_z$ in order to produce the reference circulation feeding values, which are similar to [24].

As the sampled velocity in Fig. 7a only requires the maximum and minimum velocity magnitudes to validate the numerical simulation, the orientation of the sampling lines does not change the results. However, the sampling lines here have been set at an angle to better illustrate the shear-layer thickness. The sampled shear-layer velocities u_{eff}/U_∞ are shown in Fig. 8a, whereas the vorticity fluxes $u_x\omega_z$ are shown in Fig. 8b. The integral of both the velocity profile and the vorticity flux is insensitive to sampling position because the shear layer shown in Fig. 8b is merely translated away from the wing surface as you progress in the streamwise direction, whereas its magnitude and shape are unchanged. The modeled outer shear-layer velocity is lower than the measured value of $u_{\text{eff}}/U_\infty = 1.27$, which results in a lower shear-layer feeding rate in the model than that measured. Furthermore, the measured inner shear-layer velocity of $u_i \approx 0$ confirms the assumption used in Sec. II of a negligible inner velocity. This modeled velocity gives a shear-layer feeding of

$$\frac{\partial \Gamma}{\partial t} \approx \frac{1}{2} U_\infty^2 = 0.383 \text{ m}^2/\text{s}^2 \tag{10}$$

following Eq. (4). Meanwhile, the measured vorticity flux at the most upstream sample location gives a similar value:

$$\frac{\partial \Gamma}{\partial t} = \int_0^d u_x \omega_z \, \mathrm{d}\xi = 0.431 \text{ m}^2/\text{s}^2 \tag{11}$$

where ξ is the shear-layer coordinate. This result shows that the shear-layer feeding model predicts circulation feeding in this case to

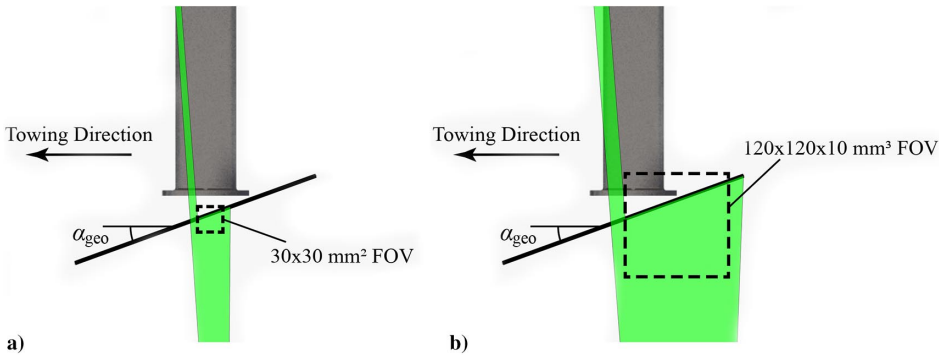

Fig. 6 Illustrations of a) the single-camera PIV FOV used to measure the shear-layer velocities and b) the four-camera 4-D-PTV FOV used to measure the large-scale flow.

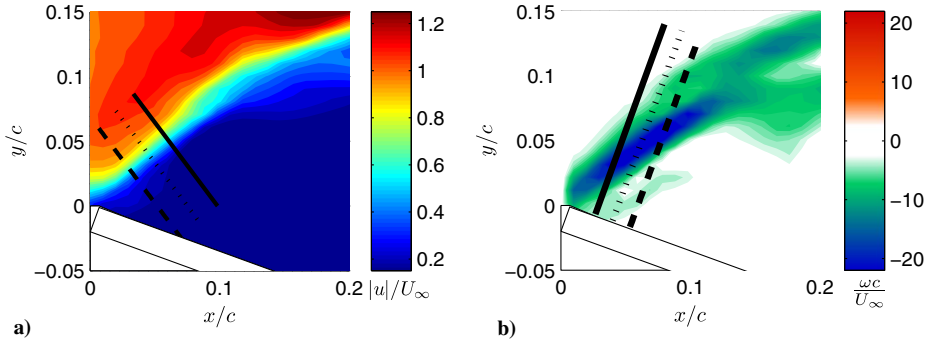

Fig. 7 Shear-layer sampling planes for a) velocity and b) vorticity.

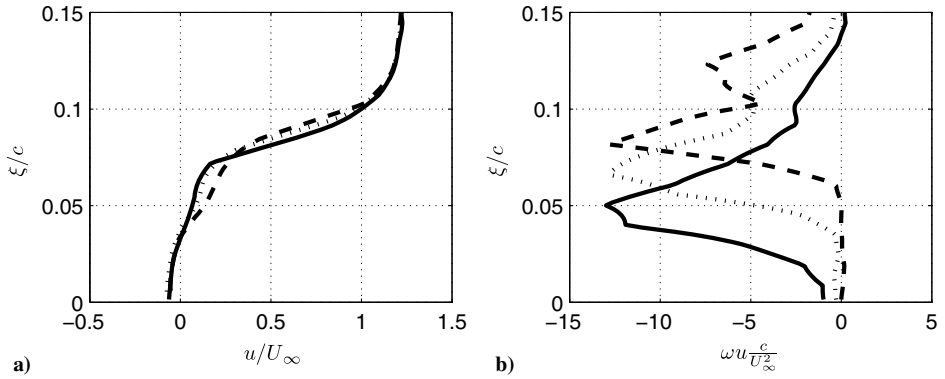

Fig. 8 Shear-layer a) velocity and b) vorticity sampled on the planes in Fig. 7.

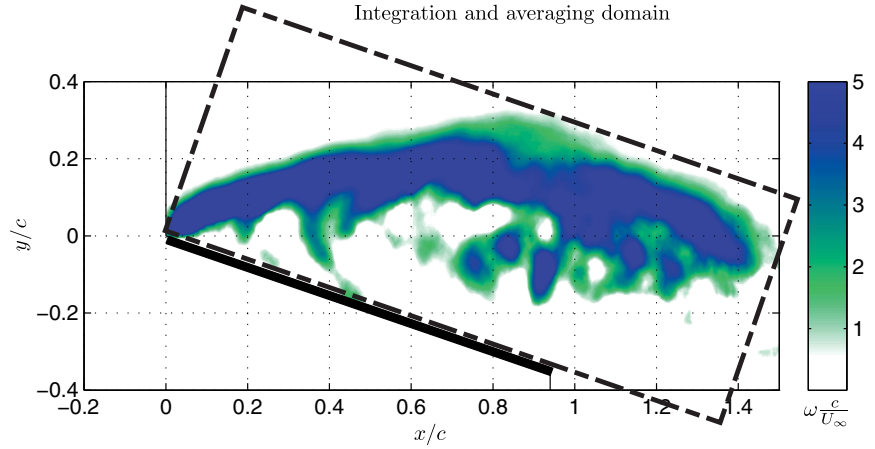

Fig. 9 Three-dimensional vorticity field, as measured with 4-D-PTV, projected into a single plane.

approximately 10% while avoiding the explicit use of the shear-layer thickness.

To compute integral circulation transport properties, 4-D-PTV data are recast into a plate-fixed frame of reference. Those 4-D-PTV data are visualized by the z-vorticity field in Fig. 9. It should be noted that, although Fig. 9 appears to be two-dimensional, this is only a projection of three-dimensional data, such that the entire velocity-gradient tensor and the gradient of circulation can be resolved directly. A single investigation window, indicated by the dashed box in Fig. 9, is used as both an integration domain and as an averaging window in order to compute circulation transport properties, as tabulated in Table 1.

The model underestimates the shear-layer feeding rate because the assumed shear-layer velocity of $u_0 = U_\infty$ is an underestimate. This is reflected in the underestimation of circulation because the two parameters are proportional. Therefore, in future work, it may be possible to improve the presented numerical method by including an improved estimate of the shear-layer velocity.

By replacing the assumed shear-layer feeding rate of $(1/2)U_\infty^2$ with the empirical feeding rate of $\partial\Gamma/\partial t = 0.43\ \mathrm{m}^2/\mathrm{s}^2$ in the model, we can estimate the sensitivity of the proposed model to errors in estimating the feeding rate, and therefore determine the value of improving circulation feeding models. Using an empirical circulation feeding value of $\partial\Gamma/\partial t = 0.43\ \mathrm{m}^2/\mathrm{s}^2$, the modeled circulation is $0.239\ \mathrm{m}^2/\mathrm{s}$, or approximately 9% greater than the measured values. This value coincides with the residual of 9% observed in the measured case. The residual of the circulation balance, tabulated in the final column of Table 1, is defined as the difference between the circulation fed into the LEV through the leading-edge shear layer and the circulation leaving the domain due to vorticity advection ($w(\partial\gamma/\partial z)$) determined from 4-D-PTV measurements. This difference is expressed as a percentage of the circulation fed into the LEV. In the modeled case, the residual of 0.1% represents a small numerical error due to the discretization of mass into particles as part of the numerical method. However, the larger 9% value measured on the delta wing is more significant because it suggests that a proportion of circulation that enters the LEV through the leading-edge shear layer is not being advected downstream, due either to the vorticity being tilted out of the measurement plane, reducing the in-plane circulation measurement, or by vorticity annihilation from the surface of the profile. If this residual is due in part to vorticity annihilation, the magnitude of annihilation that we observe here is significantly less than that reported in previous studies [24]. However, vorticity annihilation is also observed to decrease with increasing Reynolds number, and this prior study was conducted at a Reynolds number approximately an order of magnitude smaller than in the current study [24]. However, this 9% difference may also be from other sources (such as vortex tilting), and its relationship to vorticity annihilation is speculative. As the model proposed here is intended for extremely low-cost early estimates, such as for rapid parameter studies or flow control, this 9% error is within the commonly accepted tolerance. Therefore, the proposed numerical simulation represents an extremely low-cost and versatile model, which is easily applied to unsteady problems and rotating wings.

Table 1 Characteristic vortex properties for the flat-plate delta wing

	Γ, $\mathrm{m}^2/\mathrm{s}^2$	w, m/s	Shear-layer feeding, m^2/s	$\partial\Gamma/\partial z$, m/s	Residual, %
Measured	0.220	0.33	0.431	1.19	9
Modeled	0.190	0.31	0.383	1.24	0.1

V. Conclusions

In this study, a low-order model is proposed to predict the time-resolved circulation of an leading-edge vortex (LEV) in the presence of spanwise flow. This low-order model is limited to cases in which vortex tilting and viscous diffusion are small, such as that on a delta wing. This model is a numerical simulation of a vorticity-containing mass advected along the span of the profile. A priori knowledge required to successfully implement this model is limited to the wing profile shape, kinematics, and the freestream velocity. This kinematic model frees the analysis from using empirical data on the shear-layer velocity or thickness, or circulation gradients, in order to compute the circulation distribution.

This model is applied to the stationary LEV above a flat-plate delta wing, which is deemed as a canonical case to function as a proof of concept the numerical simulations. When the real feeding rate is applied to the modeled case, the predicted circulation is 9% above the measured value, which is precisely the quantity of circulation annihilated or tilted out of the measurement plane in the physical case. Furthermore, this improved circulation estimate validates each of the assumptions made about circulation transport in Sec. II. In particular, it is shown that circulation is indeed advected with the vorticity-containing mass along the span of the profile; in addition, both vortex tilting and vorticity diffusion are minimal at higher Reynolds numbers, as tested here.

Approximately 9% of the circulation entering the flat-plate delta wing is not transported out of the LEV through circulation advection. As the numerical simulation neglects viscous diffusion, vorticity annihilation, and vortex tilting, this residual value may be difficult to account for without dramatically changing the modeling formulation. However, this 9% is also within the range of early engineering estimates, before the use of high-fidelity methods. As such, the proposed model provides an attractive and extremely low-cost platform for investigating the time- and spanwise-resolved circulation distribution within an LEV on planforms of complex shape and/or undergoing unsteady motion as found in biological and biomimetic swimming and flying.

Acknowledgment

The authors would like to thank the Natural Sciences and Engineering Research Council of Canada for funding in support of this work.

References

[1] Ellington, C. P., van den Berg, C., Willmott, A. P., and Thomas, A. L. R., "Leading-Edge Vortices in Insect Flight," *Nature*, Vol. 384, No. 6610, 1996, pp. 626–630. doi:10.1038/384626a0

[2] Videler, J. J., Stamhuis, E. J., and Povel, G. D. E., "Leading-Edge Vortex Lift Swifts," *Science*, Vol. 306, No. 5703, 2004, pp. 1960–1962. doi:10.1126/science.1104682

[3] Borazjani, I., and Daghooghi, M., "The Fish Tail Motion Forms an Attached Leading Edge Vortex," *Proceedings of the Royal Society B*, Vol. 280, No. 1756, 2013, Paper 20122071. doi:10.1098/rspb.2012.2071

[4] Polhamus, E. C., "A Concept of the Vortex Lift of Sharp-Edge Delta Wings Based on a Leading Edge Suction Analogy," NASA TN D-3767, 1966.

[5] Rival, D. E., Kriegseis, J., Schaub, P., Widmann, A., and Tropea, C., "Characteristic Length Scales for Vortex Detachment on Plunging Profiles with Varying Leading-Edge Geometry," *Experiments in Fluids*, Vol. 55, No. 1, 2014, pp. 1–8. doi:10.1007/s00348-013-1660-x

[6] Rival, D. E., Prangemeier, T., and Tropea, C., "The Influence of Airfoil Kinematics on the Formation of Leading-Edge Vortices in Bio-Inspired Flight," *Experiments in Fluids*, Vol. 46, No. 5, 2009, pp. 823–833. doi:10.1007/s00348-008-0586-1

[7] Baik, Y. S., Bernal, L. P., Granlund, K., and Ol, M. V., "Unsteady Force Generation and Vortex Dynamics of Pitching and Plunging Aerofoils," *Journal of Fluid Mechanics*, Vol. 709, Oct. 2012, pp. 37–68. doi:10.1017/jfm.2012.318

[8] Widmann, A., and Tropea, C., "Parameter Influencing Vortex Growth and Detachment on Unsteady Aerodynamic Profiles," *Journal of Fluid Mechanics*, Vol. 773, June 2015, pp. 432–459. doi:10.1017/jfm.2015.259

[9] Wong, J. G., and Rival, D. E., "Determining the Relative Stability of Leading-Edge Vortices on Nominally Two-Dimensional Flapping Profiles," *Journal of Fluid Mechanics*, Vol. 766, March 2015, pp. 611–625. doi:10.1017/jfm.2015.39

[10] Onoue, K., and Breuer, K. S., "Vortex Formation and Shedding from a Cyber-Physical Pitching Plate," *Journal of Fluid Mechanics*, Vol. 793, April 2016, pp. 229–247. doi:10.1017/jfm.2016.134

[11] Ramesh, K., Gopalarathnam, A., Granlund, K., Ol, M. V., and Edwards, J. R., "Discrete-Vortex Method with Novel Shedding Criterion for Unsteady Aerofoil Flows with Intermittent Leading-Edge Vortex Shedding," *Journal of Fluid Mechanics*, Vol. 751, July 2014, pp. 500–538. doi:10.1017/jfm.2014.297

[12] Hemati, M. S., Eldredge, J. D., and Speyer, J. L., "Improving Vortex Models via Optimal Control Theory," *Journal of Fluids and Structures*, Vol. 49, Aug. 2014, pp. 91–111. doi:10.1016/j.jfluidstructs.2014.04.004

[13] Hartloper, C., and Rival, D., "Vortex Development on Pitching Plates with Lunate and Truncate Planforms," *Journal of Fluid Mechanics*, Vol. 732, Oct. 2013, pp. 332–344. doi:10.1017/jfm.2013.400

[14] Maxworthy, T., "The Formation and Maintenance of a Leading-Edge Vortex During the Forward Motion of an Animal Wing," *Journal of Fluid Mechanics*, Vol. 587, Sept. 2007, pp. 471–475. doi:10.1017/S0022112007007616

[15] Beem, H., Rival, D. E., and Triantafyllou, M. S., "On the Stabilization of Leading-Edge Vortices with Spanwise Flow," *Experiments in Fluids*, Vol. 52, No. 2, 2012, pp. 511–517. doi:10.1007/s00348-011-1241-9

[16] Panah, A. E., Akkala, J. M., and Buchholz, J. H. J., "Vorticity Transport and the Leading-Edge Vortex of a Plunging Airfoil," *Experiments in Fluids*, Vol. 56, No. 8, 2015, p. 160. doi:10.1007/s00348-015-2014-7

[17] Jain, M. V., Wong, J. G., and Rival, D. E., "A Model of Fluid-Structure-Interaction for Impulsively Started Spanwise-Flexible Wings," *Journal of Fluids and Structures*, Vol. 54, April 2015, pp. 466–478. doi:10.1016/j.jfluidstructs.2014.12.004

[18] Wong, J. G., Kriegseis, J., and Rival, D. E., "An Investigation into Vortex Growth and Stabilization for Two-Dimensional Plunging and Flapping Plates with Varying Sweep," *Journal of Fluids and Structures*, Vol. 43, Nov. 2013, pp. 231–243. doi:10.1016/j.jfluidstructs.2013.09.010

[19] Kaden, H., "Aufwicklung Einer Unstabilen Unstetigkeitsfläche," *Ingenieur-Archiv*, Vol. 2, No. 2, 1931, pp. 140–168. doi:10.1007/BF02079924

[20] Didden, N., "On the Formation of Vortex Rings: Rolling-up and Production of Circulation," *Journal of Applied Mathematics and Physics*, Vol. 30, No. 1, 1979, pp. 101–116. doi:10.1007/BF01597484

[21] Kriegseis, J., Kinzel, M., and Rival, D. E., "On the Persistence of Memory: Do Initial Conditions Impact Vortex Formation?" *Journal of Fluid Mechanics*, Vol. 736, Dec. 2013, pp. 91–106. doi:10.1017/jfm.2013.528

[22] Onoue, K., and Breuer, K. S., "A Scaling for Vortex Formation on Swept and Unswept Pitching Wings," *Journal of Fluid Mechanics*, Vol. 832, Dec. 2017, pp. 697–720. doi:10.1017/jfm.2017.710

[23] Schanz, D., Gesemann, S., and Schröder, A., "Shake-The-Box: Lagrangian Particle Tracking at High Particle Image Densities," *Experiments in Fluids*, Vol. 57, No. 5, 2016, p. 70. doi:10.1007/s00348-016-2157-1

[24] Wojcik, C. J., and Buchholz, J. H. J., "Vorticity Transport in the Leading-Edge Vortex on a Rotating Blade," *Journal of Fluid Mechanics*, Vol. 743, March 2014, pp. 249–261. doi:10.1017/jfm.2014.18

M. Green
Associate Editor